

Effect of multiple time-delay on vibrational resonance

C. Jeevarathinam,^{1,a)} S. Rajasekar,^{1,b)} and M. A. F. Sanjuán^{2,c)}

¹*School of Physics, Bharathidasan University, Tiruchirappalli 620 024, Tamil Nadu, India*

²*Nonlinear Dynamics, Chaos and Complex Systems Group, Departamento de Física, Universidad Rey Juan Carlos, Tulipán s/n, 28933 Móstoles, Madrid, Spain*

(Received 28 September 2012; accepted 8 February 2013; published online 6 March 2013)

We report our investigation on the effect of multiple time-delay on vibrational resonance in a single Duffing oscillator and in a system of n Duffing oscillators coupled unidirectionally and driven by both a low- and a high-frequency periodic force. For the single oscillator, we obtain analytical expressions for the response amplitude Q and the amplitude g of the high-frequency force at which resonance occurs. The regions in parameter space of enhanced Q at resonance, as compared to the case in absence of time-delay, show a bands-like structure. For the two-coupled oscillators, we explain all the features of variation of Q with the control parameter g . For the system of n -coupled oscillators with a single time-delay coupling, the response amplitudes of the oscillators are shown to be independent of the time-delay. In the case of a multi time-delayed coupling, undamped signal propagation takes place for coupling strength (δ) above a certain critical value (denoted as δ_u). Moreover, the response amplitude approaches a limiting value Q_L with the oscillator number i . We obtain analytical expressions for both δ_u and Q_L . © 2013 American Institute of Physics. [<http://dx.doi.org/10.1063/1.4793542>]

Time-delay is ubiquitous in many dynamical systems and the investigation of various nonlinear phenomena in time-delay systems has received a great deal of interest in recent years. In certain systems, time-delay is found to induce various phenomena which do not occur in its absence. The presence of a single time-delay is shown to alter the stability of an equilibrium point, gives birth to a limit cycle, leads to bifurcation, chaos and different types of synchronization.^{1–3} More than one time-delay is applied in certain practical systems. For example, in a laser system multi time-delays arise when it is subjected to more than one optical reflection. Therefore, it is important to analyse the effect of multi time-delay on various nonlinear phenomena. In the present work, we explore the influence of multi time-delay on vibrational resonance in the single Duffing oscillator and signal transduction in a system of n -coupled Duffing oscillators.

systems compared to single time-delayed systems. There are some notable reports on certain systems with two or three time-delayed feedback or coupling terms.^{4–11}

In recent years, much interest has been focused on the investigation of vibrational resonance with a time-delayed feedback. In a nonlinear system driven by a biharmonic force with two widely separated frequencies, the response amplitude at the low-frequency displays one or more resonance peaks when the amplitude or frequency of the high-frequency force is varied. This phenomenon is termed as *vibrational resonance*¹² and it can occur in monostable,¹³ multistable,¹⁴ and excitable¹⁵ systems. The features of vibrational resonance in the presence of a single time-delayed feedback have been analysed in the Langevin equation,¹⁶ two-coupled overdamped anharmonic oscillators,¹⁷ underdamped and overdamped Duffing oscillators,¹⁸ FitzHugh–Nagumo neuronal model,¹⁹ a genetic toggle-switch,²⁰ and a system of n -coupled bistable oscillators.²¹

Consider the multi time-delayed feedback (MTDF) of the form $(\gamma/L)\sum_{l=1}^L x(t - \tau_l)$. The feedback is γ times the average value of a finite number of delay terms. τ_l can be equally spaced or position dependent or time-dependent (modulated) or randomly/uniformly distributed over an interval. Among these, the choice of equally spaced delays is the simplest one. In this case, the feedback takes the form of $(\gamma/L)\sum_{l=1}^L x(t - l\alpha)$, where α is the lowest delay. The effect of this feedback term on stochastic resonance in a typical Langevin equation has been studied by Li and Zeng.²² The bit error rate used to quantify the output of the system is found to decrease with the increase in the value of L . Moreover, the noise intensity at which resonance occurs is found to increase with L . MTDF has also been considered in controlling of dynamics⁴ and in a photonic neuromorphic processor.¹¹ However, vibrational resonance with MTDF has

I. INTRODUCTION

In many dynamical systems, the existence of a time-delay constitutes an important fundamental feature. The time-delay often occurs because of a finite propagation time of transport of information and energy, finite reaction times, finite switching speed of amplifiers, memory effects, etc.^{1–3} Most of the works on delayed differential systems have been focused on the analysis of a single time-delay feedback. Here, we consider of interest to analyse the effect of multiple time-delay as a generalization of a single time-delay. Furthermore, higher complexity of dynamics can be realizable in multi time-delayed

^{a)}Electronic address: c.jeeva1987@gmail.com.

^{b)}Electronic address: rajasekar@cnld.bdu.ac.in.

^{c)}Electronic address: miguel.sanjuan@urjc.es.

not yet been studied. Consequently, the main objective of our present paper is to investigate how multiple delays influence the vibrational resonance in a single Duffing oscillator and weak signal transduction in a unidirectionally coupled system of n Duffing oscillators. Our main goal is to explore the enhancement of the response amplitude by the MTDf.

The Duffing oscillator is widely used as a model for many mechanical systems, optoelectronic devices, and other physical systems. Moreover, an analog simulation can be easily performed. Simple mechanical models with two stable and one unstable equilibrium states are described in Refs. 23 and 24. In these models, a steel beam is clamped to a rigid framework. If the framework is not sufficiently rigid, then it will be distorted by the oscillation of the beam. The influence of this distortion on the motion of the steel beam can be treated as a time-delayed feedback. This time-delayed feedback can be converted into a MTDf by means of an appropriate feedback device. This type of delayed feedback can be implemented in optoelectronic equipments by a field programmable gate array¹¹ and in electronic circuits using number of delay circuits proposed in Refs. 25–27. One can also treat the MTDf as an external force.

The organization of the paper is as follows. In Sec. II, we consider the single Duffing oscillator with a MTDf and driven by the biharmonic force given by

$$\ddot{x} + d\dot{x} + \omega_0^2 x + \beta x^3 + \frac{\gamma}{L} \sum_{l=1}^L x(t - l\alpha) = f \cos \omega t + g \cos \Omega t, \tag{1}$$

where $\Omega \gg \omega$. Assuming $x(t) = X(t) + \psi(t, \tau = \Omega t)$, we find an equation of motion for the slow variable $X(t)$. From the solution of its linear version, we obtain an analytical expression for the response amplitude Q and using it, we analyse the effect of MTDf on vibrational resonance. We denote Q_{\max} as the maximum value of Q at resonance when the control parameter g is varied. In $(\gamma - \alpha)$ parameter space, we identify the regions for which $Q_{\max}(\gamma) > Q_{\max}(\gamma = 0)$ for a few fixed values of L . It has a band-like structure and the number of bands is L . We obtain the condition on γ for single and double resonance and the analytical expression for g at which resonance occurs. We analyse the effect of L on resonance.

In Sec. III, first for the n -coupled Duffing oscillators whose equations read

$$\ddot{x}_1 + d\dot{x}_1 + \omega_0^2 x_1 + \beta x_1^3 = f \cos \omega t + g \cos \Omega t, \tag{2a}$$

$$\ddot{x}_i + d\dot{x}_i + \omega_0^2 x_i + \beta x_i^3 = \frac{\delta}{L} \sum_{l=1}^L x_{i-1}(t - l\alpha), \tag{2b}$$

where $i = 2, 3, \dots, n$ we express Q_i in terms of Q_{i-1} except for the first oscillator. Then, we focus our analysis on the influence of multi time-delayed coupling (MTDC) on vibrational resonance in two-coupled oscillators. When $L = 1$, the analytical expression of Q_2 (as well as $Q_i, i > 1$ for n -coupled oscillators) is independent of the time-delay α implying that the response amplitude does not change with

the time-delay. For all values of $L > 1$, Q_2 is always less than Q_1 for $g < g_{c1}$, where g_{c1} is the value of g at which the effective potential of X of the first oscillator undergoes a transition from bistability to monostability. For $g > g_{c1}$, $Q_2 > Q_1$ for certain ranges of values of α . We account these results and explain the mechanism of resonance in the first and second oscillators. We identify the regions in $(g - \alpha)$ parameter space where $Q_2 > Q_1$, for a few fixed values of δ and L . Section IV is devoted to the analysis of signal propagation in the system of n -coupled oscillators with $n = 200$. The difference between the theoretical Q_i and the numerically computed Q_i is very large for $i \gg 1$. This is due to the neglect of nonlinear terms in the equation of motion of the slow variable. Inclusion of nonlinear terms leads to a set of coupled polynomial equations for Q_i . The Q_i s obtained by solving this set of equations are in very good agreement with the numerically calculated Q_i . The coupled system exhibits undamped signal propagation (that is, $Q_{200} > Q_1$) for certain range of values of α and δ . In the undamped signal propagation, Q_i increases with i and then attains a saturation, that is, $Q_i \rightarrow Q_L$ for sufficiently large i . We obtain an analytical expression for the limiting value of Q , Q_L , and the critical value of δ , δ_u , above which undamped signal propagation takes place. Interestingly, both Q_L and δ_u are found to be independent of the parameter g . Finally, Sec. V contains conclusions.

II. SINGLE DUFFING OSCILLATOR

The main objective of this section is to obtain an expression for the response amplitude Q for the single Duffing oscillator system (1).

A. Theoretical expression for the response amplitude Q

For $\Omega \gg \omega$, let us seek the long time solution of Eq. (1) as $x(t) = X(t) + \psi(t, \tau = \Omega t)$, where X and ψ are the slow motion with period $2\pi/\omega$ and the fast motion with period $2\pi/\Omega$, respectively, and the mean value of ψ is $\langle \psi \rangle = (1/2\pi) \int_0^{2\pi} \psi \, d\tau = 0$. Substitution of $x = X + \psi$ in Eq. (1) gives the following equations for X and ψ :

$$\begin{aligned} \ddot{X} + d\dot{X} + (\omega_0^2 + 3\beta \langle \psi^2 \rangle)X + \beta(X^3 + \langle \psi^3 \rangle) + 3\beta X^2 \langle \psi \rangle \\ + \frac{\gamma}{L} \sum_{l=1}^L X(t - l\alpha) = f \cos \omega t, \end{aligned} \tag{3a}$$

$$\begin{aligned} \ddot{\psi} + d\dot{\psi} + \omega_0^2 \psi + 3\beta X^2(\psi - \langle \psi \rangle) + 3\beta X(\psi^2 - \langle \psi^2 \rangle) \\ + \beta(\psi^3 - \langle \psi^3 \rangle) + \frac{\gamma}{L} \sum_{l=1}^L \psi(\Omega t - l\alpha\Omega) = g \cos \Omega t. \end{aligned} \tag{3b}$$

Because ψ is a fast variable, one can neglect the nonlinear terms in Eq. (3b). The resulting equation for ψ is a damped and periodically driven linear equation with a linear multiple time-delayed feedback term. Its solution in the limit of $t \rightarrow \infty$ is given by

$$\psi = \mu \cos(\Omega t + \phi), \tag{4a}$$

where $\mu = g/k$,

$$k = \sqrt{\left(\Omega^2 - \omega_0^2 - \frac{\gamma}{L} \sum_{l=1}^L \cos l\alpha\Omega\right)^2 + \left(d\Omega - \frac{\gamma}{L} \sum_{l=1}^L \sin l\alpha\Omega\right)^2} \tag{4b}$$

and

$$\phi = \tan^{-1} \left(\frac{d\Omega - \frac{\gamma}{L} \sum_{l=1}^L \sin l\alpha\Omega}{\Omega^2 - \omega_0^2 - \frac{\gamma}{L} \sum_{l=1}^L \cos l\alpha\Omega} \right). \tag{4c}$$

The above solution gives $\langle \psi \rangle = 0$, $\langle \psi^2 \rangle = \mu^2/2$ and $\langle \psi^3 \rangle = 0$. Then, the equation for the slow variable X , Eq. (3a), takes the form

$$\ddot{X} + d\dot{X} + C_1X + \beta X^3 + \frac{\gamma}{L} \sum_{l=1}^L X(t - l\alpha) = f \cos \omega t, \tag{5}$$

where $C_1 = \omega_0^2 + \frac{3}{2}\beta\mu^2$. Slow oscillations occur around the equilibrium points $X_0^* = 0, X_{\pm}^* = \pm \sqrt{-(C_1 + \gamma)/\beta}$.

We introduce for convenience the change of variable $Y = X - X^*$ and obtain

$$\ddot{Y} + d\dot{Y} + \omega_r^2 Y + 3\beta X^* Y^2 + \beta Y^3 + \frac{\gamma}{L} \sum_{l=1}^L Y(t - l\alpha) = f \cos \omega t, \tag{6}$$

where $\omega_r^2 = C_1 + 3\beta X^{*2}$, which is the resonant frequency of the low-frequency oscillation in the presence of $f \cos \omega t$. For $|f| \ll 1$ and in the limit $t \rightarrow \infty$, assume that $|Y| \ll 1$ and neglect the nonlinear terms in Eq. (6). Then in the limit $t \rightarrow \infty$, the solution of Eq. (6) is $Y = Qf \cos(\omega t + \theta)$, where the response amplitude Q and the phase θ are given by

$$Q = \frac{1}{\sqrt{S}}, \quad S = \left(\omega_r^2 - \omega^2 + \frac{\gamma}{L} \sum_{l=1}^L \cos l\alpha\omega\right)^2 + \left(d\omega - \frac{\gamma}{L} \sum_{l=1}^L \sin l\alpha\omega\right)^2 \tag{7}$$

and $\theta = \phi(\Omega = \omega, \omega_0^2 = \omega_r^2)$.

B. Resonance analysis

To verify the theoretical treatment, we numerically integrate Eq. (1) using the Euler method and compute the sine and cosine components Q_s and Q_c from the equations

$$Q_s = \frac{2}{nT} \int_0^{nT} x(t) \sin \omega t dt, \tag{8a}$$

$$Q_c = \frac{2}{nT} \int_0^{nT} x(t) \cos \omega t dt, \tag{8b}$$

where $T = 2\pi/\omega$ and n is say, 500. Then, $Q = \sqrt{Q_s^2 + Q_c^2}/f$. We fix the values of the parameters as $d=0.5, \omega_0^2 = -1, \beta = 0.1, f=0.1, \omega = 1$, and $\Omega = 10$. Figure 1 shows both theoretically and numerically computed response amplitude Q versus the control parameter g for $L=1, 2, 3$, and 5 for $\gamma = 0.3$ and for two values of α . The result for $\gamma = 0$ is also shown in this figure in order to illustrate the influence of the MTDf. Vibrational resonance is observed for all the values of L chosen in our study. The theoretical Q value is in good agreement with the numerical Q value. In Fig. 1, for each value of L two values of α are chosen in such a way that for one value $Q_{\max}(\gamma) > Q_{\max}(\gamma = 0)$ (the value of Q at resonance) while for the other value $Q_{\max}(\gamma) < Q_{\max}(\gamma = 0) = 2$.

For $\gamma = 0.3$ and $\alpha = 2.6, Q_{\max}$ is >2 for odd values of L , while it is <2 for even values of L and the opposite result occurs for $\alpha = 3.4$ (not shown in Fig. 1). In view of this, using the theoretical expression of Q , we calculate the gain factor $G = Q_{\max}(\gamma)/Q_{\max}(\gamma = 0)$ and plot $G(> 1)$ as a function of γ and α for a few fixed values of L . We choose $\gamma \in [-0.4, 0.4]$ and $\alpha \in [0, 2\pi/\omega]$ with $\omega = 1$. The result is presented in Fig. 2. In this figure, $G > 1$ and $G < 1$ in the shaded and unshaded regions, respectively, on the $(\gamma - \alpha)$ plane.

For both $\gamma < 0$ and $\gamma > 0$, Fig. 2 contains L bands (shaded regions) where $G > 1$. The width of these bands is unequal. The shaded bands of $\gamma < 0$ become the unshaded bands of $\gamma > 0$. From the theoretical expression of Q , the condition for the enhanced response at resonance due to the MTDf term is $\gamma \sum_{l=1}^L \sin l\alpha\omega > 0$. This condition is realized in the shaded regions in Fig. 2. Figure 3 shows the intervals of α where $Q_{\max}(\gamma) > Q_{\max}(\gamma = 0)$ versus L for $\gamma > 0$. The intervals are independent of γ . For each value of L , the total length of α intervals in Fig. 3 is $\approx \pi$.

For wide ranges of α and γ , the gain factor is >2 , that is, the delay is able to increase the value of Q at resonance more

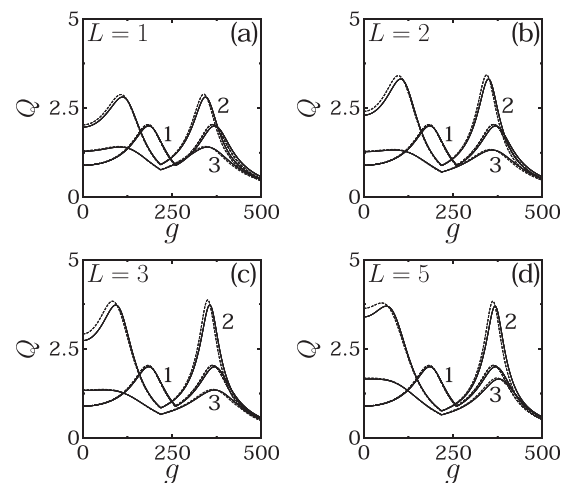


FIG. 1. Variation of the response amplitude Q with the parameter g for a few fixed number of time-delayed feedback terms. The values of the parameters are $d=0.5, \omega_0^2 = -1, \beta = 0.1, f=0.1, \omega = 1$, and $\Omega = 10$. The continuous and dashed lines are the theoretically and numerically calculated values of Q , respectively. In all the subplots, the curve 1 corresponds to $\gamma = 0$. For the curves 2 and 3, the value of γ is 0.3. The values of α for the curves 2 and 3 are 0.5 and 5.5, respectively.

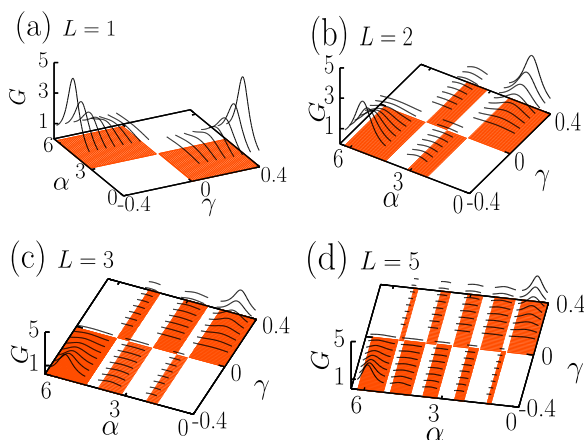


FIG. 2. Plot of $G = Q_{\max}(\gamma)/Q_{\max}(\gamma = 0) > 1$ versus γ and α for various values of L . On the $(\gamma - \alpha)$ plane, $G > 1$ in the shaded portions while $G < 1$ in the unshaded portions. The curves in the shaded regions show the variation of G with α for a few fixed values of γ .

than twice the value of Q in its absence. The addition of more and more delay terms decreases the maximum value of G . Moreover, it produces new regions with $G > 1$ in the $(\gamma - \alpha)$ parameter space and decreases the value of G to less than 1 in certain regions where $G > 1$ earlier. Also, we identify the regions in $(g - \alpha)$ parameter space where $Q(\gamma) > Q(\gamma = 0)$. Here, again we notice that the number of isolated regions where an enhanced response is realized due to the time-delay increases when the number of time-delayed feedback terms increases.

In the single oscillator, an amplification of a low-frequency signal can be achieved for a range of amplitude and frequency of the high-frequency force in the absence of time-delayed feedback. In this case, the maximum value of Q is $1/(d\omega)$. When the MTDf is introduced, we find $Q_{\max} = 1/|d\omega - (\gamma/L)\sum_{l=1}^L \sin l\alpha\omega|$. That is, Q_{\max} can be further increased or decreased by appropriate choices of γ , α , and L . Thus, the MTDf can be used to control the value of Q_{\max} .

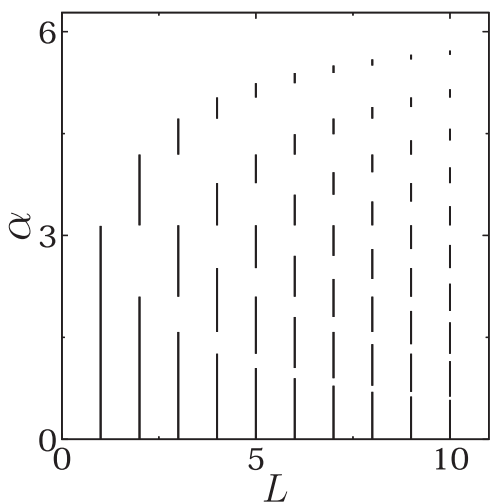


FIG. 3. Plot of intervals of α for which $Q_{\max}(\gamma > 0, \alpha) > Q_{\max}(\gamma = 0)$ as a function of L with $\omega = 1$. In the remaining intervals of α , we realize $Q_{\max}(\gamma < 0, \alpha) > Q_{\max}(\gamma = 0)$.

C. Determination of the value of g at which resonance occurs

The number of resonances in the system (1) is not always 2. In the absence of MTDf term, either one resonance or two resonances can be realized depending upon the values of the parameters ω_0^2 and β . From the theoretical expression of Q , we analyse the effect of time-delay on the values of g , denoted as g_{VR} , at which resonance occurs and the number of resonances.

In the presence of a feedback term and a biharmonic force, slow oscillations take place around the equilibrium points X_{\pm}^* or X_0^* . For $g < g_c$ where

$$g_c = \left[\frac{2k^2}{3\beta} (|\omega_0^2| - \gamma) \right]^{1/2}, \quad |\omega_0^2| - \gamma > 0 \quad (9)$$

there are three equilibrium points. $X_0^* = 0$ is the only equilibrium point for $g > g_c$. At $g = g_c$, the effective potential of X undergoes a transition from a double-well to a single-well. Equation (7) implies that Q becomes maximum when the quantity S becomes minimum. Therefore, when g is a control parameter, the value of g at which a resonance occurs corresponds to $dS/dg = 0$ or to a local minimization of ω_r^2 . The choice $dS/dg = 0$ requires

$$\omega_r^2 = \omega^2 - \frac{\gamma}{L} \sum_{l=1}^L \cos l\alpha\omega. \quad (10)$$

From this resonance condition, one can obtain an analytical expression for g_{VR} .

Case 1: $\gamma < 0$

When

$$\gamma < 0, \quad |\gamma| < |\gamma_{c<}| = \frac{\omega^2}{1 - \frac{1}{L} \sum_{l=1}^L \cos l\alpha\omega}, \quad (11)$$

a resonance occurs at two values of g given by

$$g_{\text{VR}}^{(1)} = \left[\frac{k^2}{3\beta} \left(2|\omega_0^2| - \omega^2 - 3\gamma + \frac{\gamma}{L} \sum_{l=1}^L \cos l\alpha\omega \right) \right]^{1/2} < g_c, \quad (12a)$$

$$g_{\text{VR}}^{(2)} = \left[\frac{2k^2}{3\beta} \left(|\omega_0^2| + \omega^2 - \frac{\gamma}{L} \sum_{l=1}^L \cos l\alpha\omega \right) \right]^{1/2} > g_c. \quad (12b)$$

If $\gamma < 0$ and $|\gamma| > |\gamma_{c<}|$, then only one resonance is possible and the corresponding $g_{\text{VR}}^{(1)}$ is g_c , which is the bifurcation point. The two resonances for $|\gamma| < |\gamma_{c<}|$ are due to the matching of ω_r^2 with $\omega^2 - \frac{\gamma}{L} \sum_{l=1}^L \cos l\alpha\omega$ (refer to Eq. (10)), while the resonance at $g = g_c$ for $|\gamma| > |\gamma_{c<}|$ is due to the local minimization of ω_r^2 .

Case 2: $\gamma > 0$

For $\gamma > 0$, one resonance always takes place at $g = g_{\text{VR}}^{(2)}$ given by Eq. (12b) if $|\omega_0^2| > \gamma$. Another resonance occurs at $g = g_{\text{VR}}^{(1)}$ given by Eq. (12a) if

$$|\omega_0^2| > \gamma, \quad \gamma < \gamma_{c>} = \frac{2|\omega_0^2| - \omega^2}{3 - \frac{1}{L} \sum_{l=1}^L \cos l\alpha\omega}. \quad (13)$$

Both resonances are due to the resonance condition (10). For $\gamma < \gamma_{c>}$, there are two resonances, while for $\gamma > \gamma_{c>}$ there exists only one resonance (at $g_{vr}^{(2)}$ and not at g_c as in the case for $\gamma < 0$ and $|\gamma| > |\gamma_{c<}|$). We note that in the case of the system (1), in the absence from a time-delayed feedback term, there are two resonances for $2|\omega_0^2| > \omega^2$, while one for $2|\omega_0^2| < \omega^2$. In the system (1), the number of resonances for $\gamma < 0$ depends on the parameters ω, L , and α and is independent of ω_0^2, β, f , and Ω . For $\gamma > 0$, the number of resonances depends also on the parameter ω_0^2 . Thus, by suitably choosing the values of γ, α , and L , the system can be set to display either two resonances or one resonance by varying the control parameter g . That is, the number of resonances can also be varied by means of a MTDf.

III. RESONANCE IN TWO-COUPLED DUFFING OSCILLATORS WITH MULTIPLE TIME-DELAYED COUPLING

In this section, we consider the effect of a time-delayed linear one-way coupling in two-coupled Duffing oscillators given by Eq. (2) with $n=2$. In the system (2), the biharmonic periodic force is applied to the first oscillator alone. The coupling term is linear and has multiple time-delayed terms. The evolution of x_1 is independent of $x_i, i > 1$, while those of $x_i, i > 1$ depends on x_{i-1} .

A. Theoretical approach

Writing $x_i = X_i + \psi_i$, where X_i 's and ψ_i 's are slow variables and fast variables, respectively, and applying the theoretical treatment used in the previous section, we obtain the following results:

$$Y_i(t) = Q_i f \cos(\omega t + \phi_i), \quad (14)$$

where

$$Q_1 = \frac{1}{\sqrt{(\omega_{r1}^2 - \omega^2)^2 + d^2\omega^2}}, \quad Q_i = P_i Q_{i-1}, \quad (15a)$$

$$P_i = \frac{\delta r_\omega}{\sqrt{(\omega_{ri}^2 - \omega^2)^2 + d^2\omega^2}}, \quad i = 2, 3, \dots, n \quad (15b)$$

$$\omega_{ri}^2 = C_i + 3\beta X_i^{*2}, \quad C_i = \omega_0^2 + \frac{3}{2}\beta\mu_i^2, \quad i = 1, 2, \dots, n \quad (15c)$$

$$X_1^* \left(X_1^{*2} + \frac{C_1}{\beta} \right) = 0, \quad (15d)$$

$$X_i^{*3} + \frac{C_i}{\beta} X_i^* - \frac{\delta}{\beta} X_{i-1}^* = 0, \quad i = 2, 3, \dots, n \quad (15e)$$

$$\mu_1 = g/k, \quad \mu_i = \frac{\delta r_\Omega}{k} \mu_{i-1}, \quad i = 2, 3, \dots, n \quad (15f)$$

$$k = \sqrt{(\Omega^2 - \omega_0^2)^2 + d^2\Omega^2}, \quad (15g)$$

$$r_\omega = \frac{1}{L} \left[\left(\sum_{l=1}^L \sin l\alpha\omega \right)^2 + \left(\sum_{l=1}^L \cos l\alpha\omega \right)^2 \right]^{1/2} \quad (15h)$$

and r_Ω is similar to r_ω with ω replaced by Ω in Eq. (15h). We obtain an important result from the above theoretical treatment. When $L=1$, that is, the number of time-delayed terms in the coupling is only one, then Q_i and μ_i given by Eqs. (15a) and (15f), respectively, reduce to

$$Q_i = \frac{\delta}{\sqrt{(\omega_{ri}^2 - \omega^2)^2 + d^2\omega^2}} Q_{i-1}, \quad \mu_i = \frac{\delta}{k} \mu_{i-1}, \quad (16)$$

where $i = 2, 3, \dots, n$. The response amplitudes Q_i 's, $i > 2$ are independent of the time-delay parameter α . This is because when $L=1$ the coupling term $\delta x_{i-1}(t - \alpha)$ becomes $\delta X_{i-1}^* + \delta Q_{i-1} f \cos(\omega t - \omega\alpha + \phi_{i-1})$ in which $-\omega\alpha + \phi_{i-1}$ is an unimportant phase factor as far as the amplitudes of oscillation of x_i 's are concerned. The above theoretical prediction is confirmed through numerical simulation. Therefore, in the rest of our analysis, we consider $L > 1$. In the following, we study the two-coupled oscillators and consider the system of n -coupled oscillators in Sec. IV.

B. Resonance analysis

We fix the values of the parameters as $\omega_0^2 = -1, d=0.5, \beta=0.1, f=0.1, \omega=1$, and $\Omega=10$. Two slow oscillations of X_1 with the same amplitude take place around the equilibrium points $X_{1\pm}^* = \pm \sqrt{-C_1/\beta}$ for $g < g_{c1} = \sqrt{2k^2|\omega_0^2|/(3\beta)}$, while for $g > g_{c1}$ only one slow motion exists and is around $X_{10}^* = 0$. The equilibrium points around which slow oscillations of the second oscillator occur are the roots of the Eq. (15e) with $i=2$ and is a cubic equation. Analytical expression for the roots of the cubic equation of the form (15e) is given in Ref. 28. When there are three real roots of Eq. (15e), we designate them as X_{2L}^*, X_{2M}^* , and X_{2U}^* with $X_{2L}^* < X_{2M}^* < X_{2U}^*$. In this case, the effective potential of X_2 is of a double-well form. X_{2L}^* and X_{2U}^* are the local minima of left- and right-wells, respectively, around which slow motion takes place. X_{2M}^* is the local maximum of the effective potential of X_2 . When there exists only one real root, then the effective potential becomes a single-well and a slow oscillation will occur around this equilibrium state.

Figure 4 shows the regions in $(g - \alpha)$ parameter space where $Q_2 > Q_1$ for three fixed values of the coupling

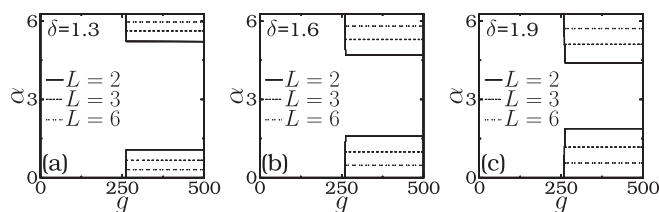


FIG. 4. Plot indicating the regions (below the lower curve and above the upper curve for each fixed values of L) in $(g - \alpha)$ parameters space where $Q_2 > Q_1$ for three fixed values of L and δ . The values of the other parameters are $d=0.5, \omega_0^2 = -1, \beta=0.1, f=0.1, \omega=1$, and $\Omega=10$.

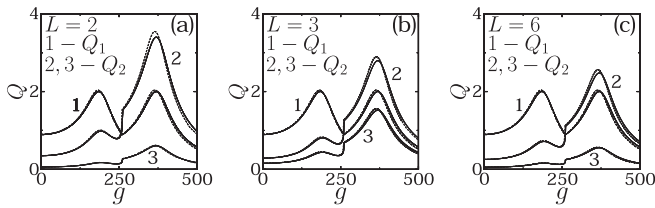


FIG. 5. Q_2 (curves 2 and 3) versus g for $L=2, 3$, and 6 and for two fixed values of α . The value of δ is 1.9 . In all the subplots, Q_1 (curve 1) is also shown to demonstrate the effect of the MTDC on Q_2 . The values of α used are: subplot (a): curve 2 (3) $-\alpha=0.1(3.5)$, subplot (b): curve 2 (3) $-\alpha=0.75(1.4)$, subplot (c): curve 2 (3) $-\alpha=0.45(0.9)$. The continuous and dashed curves are theoretically and numerically computed values of Q_2 , respectively.

strength δ and L . Q_2 is found to be greater than Q_1 for $g > g_{c1} = 261.1$ for the values of α below the lower curve and above the upper curve in Fig. 4. The intervals of α for which $Q_2 > Q_1$ increase for increasing values of δ . For further understanding of the effect of time-delay α , in Fig. 5, we plot the variation of both the theoretical Q_2 and the numerically calculated Q_2 with g for $L=2, 3$, and 6 , $\delta = 1.9$ and for two values of α .

Q_1 is also shown to compare the effect of L and α on the response amplitude Q_2 . The theoretical Q_2 is in very good agreement with the numerically computed Q_2 . In Fig. 5, whenever X_1 and X_2 have more than one equilibrium point, we used X_{1U}^*, X_{2U}^* for the calculation of Q_1 and Q_2 . The response amplitude Q_1 of the system driven by the biharmonic force has two resonance peaks. Q_2 also displays two resonance peaks. In Figs. 4(c) and 5, we notice that $Q_2 < Q_1$ for $g < g_{c1} = 261.1$, for all values of α and L . For certain values of α (lying below the lower curve and above the upper curve in Fig. 4(c)), $Q_2 > Q_1$ for $g > g_{c1}$.

Now, we explain the mechanism of the resonance and the above result for $L=2$. As g increases from 0 , we note that $X_1^*, X_2^*, \omega_{r1}^2, \omega_{r2}^2$, and P_2 given by Eq. (15) vary and hence Q_1 and Q_2 also vary. The features of Q_1 and Q_2 can be accounted from the study of the dependence of the above five quantities. Figure 6 illustrates the variation of X_1^* and X_2^* with g for $\alpha = 0.1$ and $\delta = 1.9$. In Fig. 7, we plot $\omega_{r1}^2, \omega_{r2}^2$,

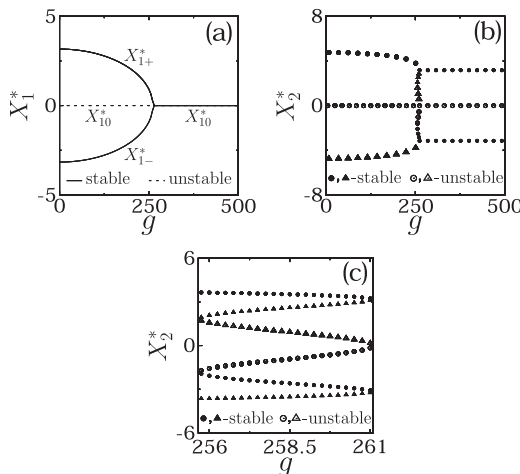


FIG. 6. (a) X_1^* versus g and (b)–(c) X_2^* versus g of the two-coupled Duffing oscillators system for $L=2, \alpha=0.1$, and $\delta=1.9$. For details, see the text.

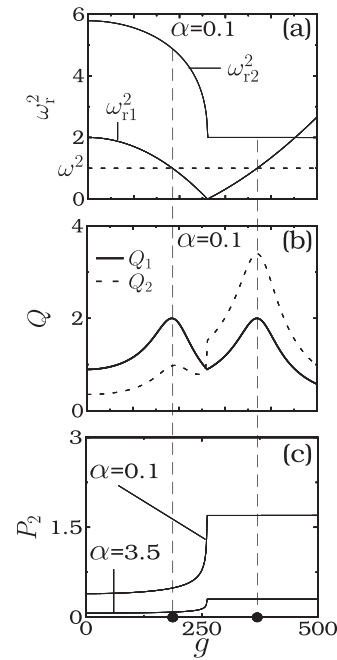


FIG. 7. (a) ω_{r1}^2 and ω_{r2}^2 , (b) Q_1 and Q_2 , and (c) P_2 versus the control parameter g for $L=2, \alpha=0.1$, and $\delta=1.9$. In the subplot (c), P_2 versus g is shown for $\alpha=3.5$ also. The two solid circles on the g -axis mark the values of g at which resonance occurs.

P_2 and also Q_1 and Q_2 as a function of g . At $g=0$, $\omega_{r1}^2 = 2|\omega_0^2|$. In Fig. 7(a), as g increases from 0 , ω_{r1}^2 decreases from $2|\omega_0^2|$, becomes zero at g_{c1} (where a bifurcation from bistability to monostability occurs as shown in Fig. 7(a)), and then increases with further increase in g . ω_{r1}^2 matches with ω^2 at two values of g and at these values Q_1 becomes maximum with the value $1/(d\omega)$. Thus, there are two resonances of Q_1 with the same value.

Next, we analyse the variation of Q_2 using its theoretical expression. First, we consider the case of $g < g_{c1} = 261.1$. The variation of Q_2 with g depends on the variation of both Q_1 and P_2 (because ω_{r2}^2 in P_2 changes with g). When $g < g_{c2} = 255.7$, then for both X_{1+}^* and X_{1-}^* (shown in Fig. 6(a)) the cubic Eq. (15e) has only one real root. In Fig. 6(b), the solid circle and the solid triangle represent X_2^* for the choices X_{1+}^* and X_{1-}^* , respectively. These two branches of X_2^* are stable while the middle branch marked by the open circle corresponding to $X_{10}^* = 0$ is unstable. The value Q_2 is the same for both X_{2+}^* and X_{2-}^* because $|X_{2-}^*| = X_{2+}^*$ and X_2^* occurs as X_2^{*2} in the expression for ω_{r2}^2 . For $g_{c2} < g < g_{c1}$, there are three equilibrium points of X_2 for both X_{1+}^* and X_{1-}^* . They are shown in Fig. 7(c). In this figure, the solid circles (solid triangles) and the open circles (open triangles) are the stable and unstable states, respectively, of X_2^* corresponding to $X_{1+}^*(X_{1-}^*)$. In Figs. 7(a) and 7(b) for the calculation of ω_{r2}^2 and Q_2 , respectively, we used the top most branch of X_2^* . When g increases from 0 as shown in Fig. 7(a), ω_{r2}^2 decreases from a value $> \omega_{r1}^2$ up to $g = g_{c1}$. For $g < g_{c1}$, ω_{r2}^2 is $> \omega^2$ and there is no matching of ω_{r2}^2 with ω^2 . There is no possibility of resonance in Q_2 by tuning ω_{r2} . In Fig. 7(c), we plot the amplification factor P_2 of Q_2 (refer Eq. (15b)). P_2 (corresponding to $\alpha = 0.1$) increases from a small value,

however, for $g < g_{c1}$ it is <1 and is almost constant except near g_{c1} . Therefore, according to Eq. (15a) $Q_2 < Q_1$ and the variation of Q_2 is similar to Q_1 . As a result, Q_2 exhibits a resonance at the value of g at which Q_1 also shows a resonance.

Now, we look at the case of $g > g_{c1}$. X_1 has only one equilibrium state ($X_{10}^* = 0$). From Eq. (15e), we obtain $X_2^* = 0, \pm\sqrt{-C_2/\beta}$. There are three equilibrium states of X_2 for the parametric values used in our study. $X_2^* = 0$ is unstable while the other two are stable. Because $\Omega^2 \gg |\omega_0^2|$, for $g > g_{c1}$ with $X_1^* = 0, X_2^* = \pm\sqrt{-C_2/\beta}$ we can approximate ω_{r2}^2 as

$$\omega_{r2}^2 \approx 2|\omega_0^2| - O(g^2/\Omega^8), \quad g > g_{c1}. \quad (17)$$

Neglecting the last term in Eq. (17), as it is very small, we get $\omega_{r2}^2 \approx 2|\omega_0^2| = 2$ and is evident in Fig. 7(a). Because ω_{r2}^2 is almost a constant, P_2 given by Eq. (15b) is also a constant. For $\alpha = 0.1$ and $\delta = 1.9$, the quantity P_2 is >1 . Consequently, $Q_2 = P_2 Q_1 > Q_1$. Further, the variation of Q_2 is again similar to Q_1 and both Q_1 and Q_2 exhibit a second resonance at a value of $g > g_{c1}$. For $\alpha = 3.5$, in Fig. 7(c) $P_2 < 1$ for the entire range of g considered and hence in Fig. 5(a) Q_2 (curve 3) is always $<Q_1$.

We note that the slow variable X_1 has bistability for $g < g_{c1} = 261.1$ and monostability for $g > g_{c1}$. For $g < g_{c1}$,

there are two co-existing orbits, one around X_{1+}^* and another one around X_{1-}^* . As g increases from a small value, the center of these orbits X_{1+}^* and X_{1-}^* moves towards the origin. For $g > g_{c1}, X_1^* = 0$ is the only equilibrium point and there exists only one slow motion and it occurs around $X_1^* = 0$. What happens for the second oscillator? When $g < g_{c2} = 255.7$, X_2 has only one equilibrium state for each X_1^* and hence the effective potential of the slow variable X_2 is monostable. Figures 8(a) and 8(b) show the numerically computed periodic orbits of the second oscillator for $g = 210$. Q_2 of the two orbits in Figs. 8(a) and 8(b) are the same. In the interval $g_{c2} < g < g_{c1}$ for both X_{1+}^* and X_{1-}^* , there are three equilibrium states of X_2 with two being stable and one becomes unstable as shown in Fig. 6(c). In the numerical simulation, we can observe four co-existing orbits depending upon the initial conditions. These co-existing orbits are displayed in Figs. 8(c)–8(f) for $g = 258$. The response amplitudes of the orbits in Figs. 8(c) and 8(d) are the same ($Q_2 = 1.10572$). The amplitudes of the orbits in Figs. 8(e) and 8(f) are also the same ($Q_2 = 2.72064$) but different from those shown in Figs. 8(c) and 8(d). For $g > g_{c1}$, X_1 has only one equilibrium state $X_{10}^* = 0$, while X_2 has three states, two of them stable. The two co-existing orbits of the second oscillator are shown in Figs. 8(g) and 8(h) for $g = 270$. Their amplitudes are the same. The point is that for $g < g_{c2}$, X_2 has a monostable state and for $g > g_{c2}$ it has bistable states.

IV. SIGNAL PROPAGATION IN A SYSTEM OF N -COUPLED OSCILLATORS

In this subsection, we investigate the signal propagation in a system of n -coupled Duffing oscillators, Eq. (2), with $n = 200$. We use $Q_{200} > Q_1$ as the criterion for undamped and enhanced signal propagation in the coupled oscillators system.

For the single and two-coupled Duffing oscillators, a theoretically calculated Q is shown to be in good agreement with the numerically computed Q . Note that in obtaining the theoretically calculated Q , we have neglected the nonlinear terms in the equations of motion of the fast variable ψ and the slow variable $Y (= X - X^*)$. In the systems of n -coupled oscillators, the error in the theoretical Q due to the above approximation grows with the oscillator number i when $Q_i > 1$ for $i \gg 1$. We define

$$\Delta Q_i = Q_{i,T} - Q_{i,N}, \quad (18)$$

where $Q_{i,T}$ and $Q_{i,N}$ represent Q_i values determined theoretically and numerically. Figure 9 shows the variation of ΔQ_i with i for $d = 0.5, \omega_0^2 = 1, \beta = 1, f = 0.1, \omega = 1.5, \Omega = 15, L = 2, \delta = 2.5, \alpha = 1$ and for three values of g .

In obtaining μ_i given by Eq. (15f), we have assumed that $\ddot{\psi}_i \gg \psi_i^2$ and ψ_i^3 . This can be valid in the case of $i = 1$, where the first oscillator is driven by the high-frequency force $g \cos \Omega t$. Because the other oscillators are not driven explicitly by the high-frequency force, the assumption $\ddot{\psi}_i \gg \psi_i^2$ and ψ_i^3 is not valid. Moreover, in the analytical calculation of Q_i also the nonlinear terms in the equations of Y_i are neglected. There are errors due to the neglect of

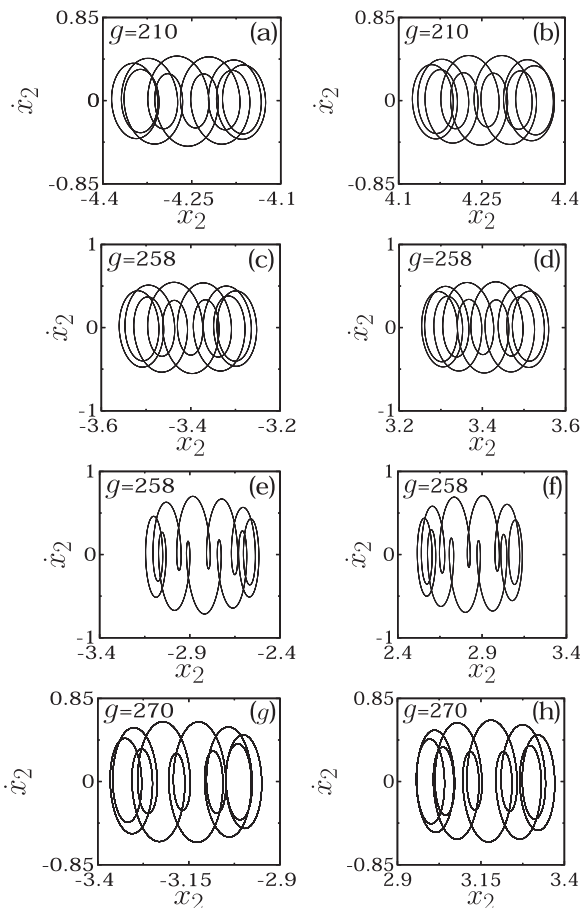


FIG. 8. Phase portraits of co-existing orbits of the second oscillator of the two-coupled Duffing oscillators for a few values of g with $L = 2, \alpha = 0.1$, and $\delta = 1.9$.

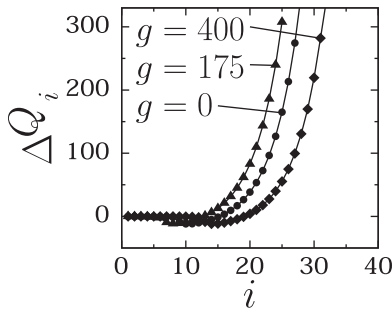


FIG. 9. ΔQ_i , difference between the theoretically calculated Q_i and the numerically computed Q_i , versus i for $d=0.5$, $\omega_0^2=1$, $\beta=1$, $f=0.1$, $\omega=1.5$, $\Omega=15$, $L=2$, $\delta=2.5$, $\alpha=1$ and for three values of g .

nonlinear terms in the equations of ψ_i and Y_i and further the errors in ψ_i and Y_i propagate to the $(i+1)$ th oscillator through the coupling term. As a result, ΔQ_i is negligible for the first few oscillators and becomes large for $i \gg 1$.

In order to minimize the error in the theoretical Q_i and also to minimize the propagation of this error through the consecutive oscillators, we include nonlinear terms in the calculation of the amplitudes of oscillation of the fast and slow variables.²⁹ We assume

$$\psi_i = \mu_i \cos(\Omega t + \phi_i), \quad X_i = A_i \cos(\omega t + \theta_i). \quad (19)$$

Substitution of the above solutions in the equations

$$\ddot{\psi}_1 + d\dot{\psi}_1 + \omega_0^2\psi_1 + \beta\psi_1^3 = g \cos \Omega t, \quad (20a)$$

$$\ddot{\psi}_i + d\dot{\psi}_i + \omega_0^2\psi_i + \beta\psi_i^3 = \frac{\delta}{L} \sum_{l=1}^L \psi_{i-1}(t - l\alpha), \quad (20b)$$

$$\ddot{X}_1 + d\dot{X}_1 + \omega_0^2X_1 + \beta X_1^3 = f \cos \omega t, \quad (20c)$$

$$\ddot{X}_i + d\dot{X}_i + \omega_0^2X_i + \beta X_i^3 = \frac{\delta}{L} \sum_{l=1}^L X_{i-1}(t - l\alpha), \quad (20d)$$

where $i = 2, 3, \dots, n$ and $\omega_{0j}^2 = \omega_0^2 + \frac{3}{2}\beta\mu_j^2$, $j = 1, 2, \dots, n$ gives

$$\mu_i^6 + a_\mu \mu_i^4 + b_\mu \mu_i^2 - R_{i\mu} = 0, \quad (21)$$

$$A_i^6 + a_{iA} A_i^4 + b_{iA} A_i^2 - R_{iA} = 0, \quad i = 1, 2, \dots, n \quad (22)$$

where

$$a_\mu = \frac{8}{3\beta}(\omega_0^2 - \Omega^2), \quad b_\mu = \frac{16}{9\beta^2}[(\omega_0^2 - \Omega^2)^2 + d^2\Omega^2], \quad (23a)$$

$$R_{1\mu} = \frac{16g^2}{9\beta^2}, \quad R_{1A} = \frac{16f^2}{9\beta^2}, \quad (23b)$$

$$a_{iA} = \frac{8}{3\beta}(\omega_{0i}^2 - \omega^2),$$

$$b_{iA} = \frac{16}{9\beta^2}[(\omega_{0i}^2 - \omega^2)^2 + d^2\omega^2], \quad i = 1, 2, \dots, n \quad (23c)$$

$$R_{i\mu} = \frac{16\delta^2 r_\Omega^2 \mu_{i-1}^2}{9\beta^2}, \quad R_{iA} = \frac{16\delta^2 r_\omega^2 A_{i-1}^2}{9\beta^2}, \quad i = 2, 3, \dots, n. \quad (23d)$$

r_ω is given by Eq. (15h) and r_Ω is obtained from r_ω by replacing ω by Ω . Equations (21) and (22) can be viewed as cubic equations for the variables μ_i^2 and A_i^2 , respectively. We determine μ_i, A_i and then $Q_i = A_i/f$ by solving Eqs. (21) and (22).

First, we check the validity of the theoretical approach. In Fig. 10(a), we plot both the theoretically calculated Q_i and the numerically computed Q_i as a function of i for three values of g with $L=2$, $\alpha=1$, and $\delta=2.5$. We notice a very good agreement of the theoretical Q_i with the numerical Q_i . For each fixed value of g as i increases, Q_i increases slowly then increases sharply to a higher value and finally it attains a saturation value. The plot of Q_i versus i displays a kink-like dependence. This implies that there are a critical number of oscillators for obtaining the maximum response and these numbers depend on the control parameters. An interesting result in Fig. 10(a) is that $Q_i > Q_1$ for $i > 1$, even in the absence of a high-frequency force. That is, a coupling alone is able to give rise to an enhanced undamped signal propagation in the coupled oscillators. Figure 10(b) shows the influence of the number of time-delay terms in the coupling on Q_i where $g=175$, $\alpha=1$, and $\delta=5$. For $L=2$ and 3, an undamped signal propagation occurs while for $L=4$ a damped signal propagation takes place.

In Fig. 10, for sufficiently large values of i , the response amplitude Q_i becomes a constant. We call this limiting or saturation value of Q_i as Q_L . Interestingly, we can determine μ_L, A_L and hence $Q_L = A_L/f$ from Eqs. (21) and (22), respectively. Substituting $\mu_i = \mu_{i-1} = \mu_L$ and $A_i = A_{i-1} = A_L$ for sufficiently large i in Eqs. (21) and (22), we obtain

$$\mu_L = 0, \quad \left\{ \frac{4}{3\beta} \left[\Omega^2 - \omega_0^2 \pm \sqrt{\delta^2 r_\Omega^2 - d^2 \Omega^2} \right] \right\}^{1/2} \quad (24)$$

and

$$A_L = 0, \quad \left\{ \frac{4}{3\beta} \left[\omega^2 - \omega_{0L}^2 \pm \sqrt{\delta^2 r_\omega^2 - d^2 \omega^2} \right] \right\}^{1/2}, \quad (25)$$

where $\omega_{0L}^2 = \omega_0^2 + \frac{3}{2}\beta\mu_L^2$. $A_L = 0$ and $\neq 0$ correspond to a damped and an undamped signal propagation, respectively. We can also find out the condition on the parameter δ for undamped signal propagation. In Fig. 10, in all the examples

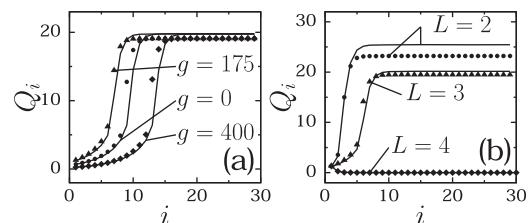


FIG. 10. Variation of Q_i with i for (a) three values of g with $L=2$, $\alpha=1$, and $\delta=2.5$ and (b) three values of L with $g=175$, $\delta=5$, and $\alpha=1$. The continuous lines and the symbols represent the theoretically and numerically computed values of Q_i , respectively.

of undamped signal propagation $Q_2 > Q_1$. This is further confirmed for a large set of parametric values. Therefore, we assume that if $Q_2 > Q_1$ then

$$Q_i \geq Q_{i-1} \geq \dots > Q_3 > Q_2 > Q_1. \tag{26}$$

For Q_1 and Q_2 , very much satisfactory analytical expressions are given by Eq. (15a) with $i=2$. The condition for $Q_2 > Q_1$ is $P_2 > 1$, where

$$P_2 = \frac{\delta r_\omega}{\sqrt{(\omega_{i2}^2 - \omega^2)^2 + d^2 \omega^2}} \tag{27a}$$

and

$$\omega_{i2}^2 = \omega_0^2 + \frac{3\beta g^2 \delta^2 r_\Omega^2}{2\Omega^8}. \tag{27b}$$

Because of the term Ω^8 , the second term in ω_{i2}^2 can be neglected. Then, $P_2 > 1$ becomes

$$\delta > \delta_u = \frac{\sqrt{(\omega_0^2 - \omega^2)^2 + d^2 \omega^2}}{r_\omega}. \tag{28}$$

We can realize undamped signal propagation for $\delta > \delta_u$. One important result from Eqs. (25) and (28) is that both A_L (that is, Q_L) and δ_u are independent of the amplitude g of the high-frequency periodic force. Figure 10(a) confirms this. In this figure, all the numerically computed Q_i for different values of g approach the same limiting value. Figure 11 shows the variation of δ_u with the number of time-delayed terms L and the time-delay α . In this figure, for clarity, only the values $\delta_u < 10$ are shown. When $\delta_u > 10$ is also considered, then the δ_u curve has L peaks for a given value of L . For δ values above the threshold curve, an undamped signal propagation occurs. For $L=2$ and $\alpha = 1, 1.5$, and 3 , the theoretical and the numerically computed values of δ_u are (1.99, 1.96), (3.38, 3.31), and (2.32, 2.30), respectively. In Fig. 12, we plot Q_L versus δ and α for four fixed values of L . The effect of the number of time-delayed terms L and the time-delay α on Q_L can be clearly seen in this figure. The dependence of Q_L on α is nonmonotonic. Even for large values of δ , there are intervals of α in which $Q_L = 0$ (damped signal propagation).

In the vibrational resonance setup, with single time-delayed coupling the dynamics of the coupled oscillators is

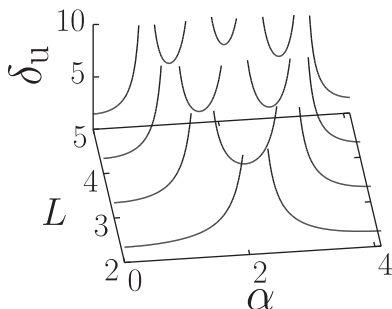


FIG. 11. Dependence of δ_u on the time-delay α and the number of time-delayed terms L . $\delta_u < 10$ are alone shown in this plot.

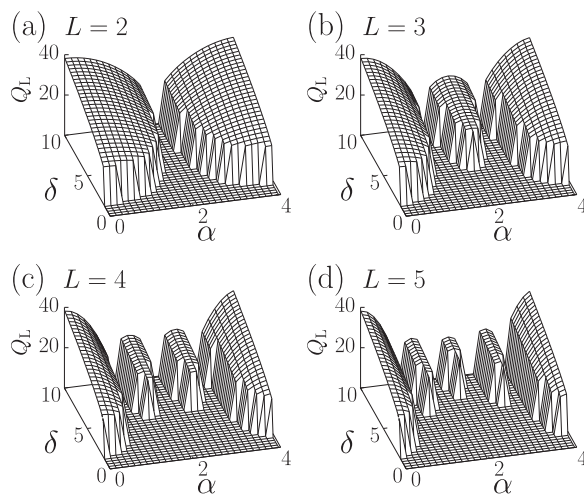


FIG. 12. Three-dimensional plot of Q_L versus δ and α for four fixed values of the number of time-delayed coupling terms. Q_L is independent of the parameter g .

independent of the delay parameter α . On the other hand, as seen in Fig. 12, the area of the regions in $(\alpha - \delta)$ parameters space where enhanced signal propagation takes place decreases with increase in the number of coupling terms. For practical applications of signal detection and amplification, two time-delayed unidirectional coupling is a better choice than single and higher number of delayed couplings.

In the n -coupled systems (2), Q_L and δ_u are independent of the control parameter g . That is, signal transduction at the low-frequency of the input signal is induced in the coupled oscillators by the coupling term and not by the high-frequency force applied to the first oscillator. However, Q_i depends on g for values of i not very large. To illustrate this in Fig. 13, we show Q_i versus i and g for $L=2$, $\delta = 2.5$ and three values of α . For $\alpha = 1$ and 3 , $\delta_u = 1.99$ and 2.32 , respectively, and hence for each fixed value of g the response amplitude $Q_i > Q_1$ for $i > 1$. For the first few number of oscillators, the response amplitude profile clearly shows the occurrence of a resonance at a value of g . For each fixed value of g , Q_i increases and attains the limiting value Q_L .

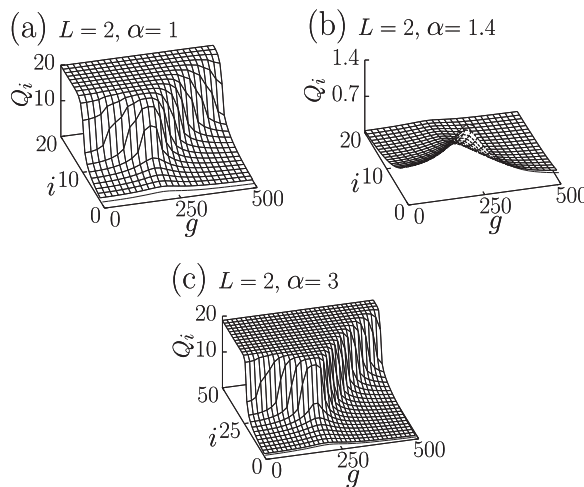


FIG. 13. Q_i versus i and g for three values of α with $L=2$ and $\delta = 2.5$. The thick line represents Q_1 .

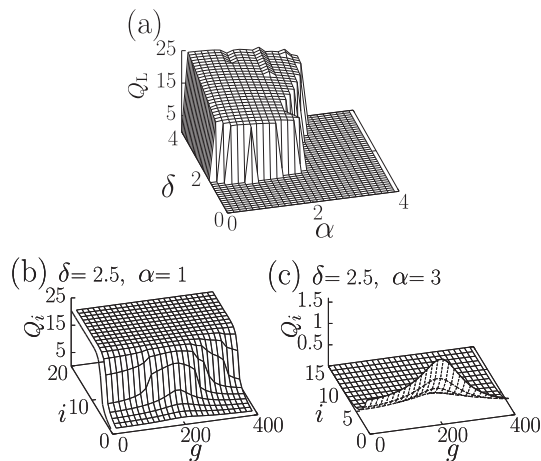


FIG. 14. (a) Q_L versus δ and α for the system of n -coupled Duffing oscillators with the ITDC. The values of the parameters are $d=0.5$, $\omega_0^2=1$, $\beta=1$, $f=0.1$, $\omega=1.5$, $\Omega=15$. Q_L is independent of the parameter g . (b)-(c) Q_i versus i and g for two values of α with $\delta=2.5$.

We notice that $Q_L \neq 0$ for $g=0$. Signal transduction takes place even in the absence of a high-frequency force. The significance of this result is that weak signal detection and amplification can be achieved either by driving a single nonlinear system by a high-frequency periodic signal or by means of sufficient number of one-way coupled oscillators without driving the oscillators by a high-frequency signal. The theoretical treatment used in the present study clearly brings out the role of the high-frequency periodic force and the MTDC on the response amplitude and signal transduction in the coupled oscillators.

In order to know whether the enhanced response of the i th oscillator at the low-frequency ω is due to the presence of the low-frequency signal in the first oscillator or the low-frequency component is induced by the time-delayed coupling, we numerically calculated $Q_i(\omega)$ for $f=0$. We found $Q_i(\omega)=0$. That is, the system responds to the low-frequency signal only when it is present in the first oscillator.

In this section, so far we have considered the system of n -coupled Duffing oscillators with MTDC. We have investigated the response of the system with integrative time-delayed coupling (ITDC) of the form $(\delta/\alpha)\int_{t-\alpha}^t x_{i-1}(\tau)d\tau$. The feedback is not only time-delayed but also cumulative over a certain time interval α . This kind of time-delay was earlier introduced in the “integrate-and-fire” models³⁰ and self-organized critically³¹ and its effect has been analysed in a neuronal model³² and in a two-coupled Landau–Stuart oscillators.³³

The theoretical treatment employed for the coupled oscillators with MTDC can be used to analyse the influence of ITDC. However, here we present very briefly our numerical simulation. In the case of ITDC, Q_L is also found to be independent of the parameter g . Figure 14(a) shows the variation of Q_L with the parameters δ and α . $Q_L > 0$ for a range of values of α and δ . The difference between the effects of ITDC and MTDC can be clearly seen by comparing Figs. 14(a) and 12. Figure 14(b) depicts the dependence of Q_i on g for $\delta=2.5$ and $\alpha=1$ for which an undamped signal transduction takes place. In the case of ITDC also resonance

occurs only for first few oscillators. Figure 14(c) shows an example of decay of Q_i with i where $\delta=2.5$ and $\alpha=3$.

V. CONCLUSIONS

We have presented the analysis of high-frequency periodic force induced vibrational resonance in a single Duffing oscillator with MTDF and signal propagation in a system of n -coupled Duffing oscillators with multi-time delayed unidirectional coupling. Various nontrivial results are obtained through a theoretical treatment. In the single oscillator, when the amplitude g of the high-frequency periodic force is varied, a single or a double resonance occurs depending upon the values of the parameters ω_0^2 , ω , α , L , and γ and is independent of the parameters d , f , β , and Ω . In the γ (the strength of feedback term)– α (time-delay) parameter space, the regions with $Q_{\max}(\gamma) > Q_{\max}(\gamma=0)$ have L bands, where L is the number of time-delayed feedback terms. The maximum value of response amplitude is found to decrease when the number of feedback terms increases. The response amplitude Q depends on all the parameters except f (the analysis performed in the present work is valid only for $|f| \ll 1$) while its value at resonance depends on the parameters d , ω , γ , α , and L .

The theoretical treatment allows us to determine (i) the mechanism of resonance, (ii) the number of resonances, (iii) analytical expression for control parameters at which resonance occurs, (iv) the maximum value of response amplitude, and (v) the regions in the parameters space where an enhanced response occurs due to MTDF.

More importantly, the theoretical approach is able to determine and explain the various features of signal propagation in coupled oscillators. One interesting prediction is that in coupled oscillators the response amplitude as well as the dynamics is independent of the time-delay parameter α when the number of coupling terms is only one. The system exhibits undamped signal propagation for appropriate choices of the parameters and these choices of parameters can be determined from the theoretical approach. We wish to stress that in the coupled oscillators system (2), even though only the first oscillator is driven by the high-frequency periodic force, fascinating results on signal propagation are obtained by the action of the unidirectional coupling with multiple time-delayed terms.

ACKNOWLEDGMENTS

C.J. expresses his gratitude to University Grants Commission (UGC), India for the financial support in the form of UGC meritorious fellowship. M.A.F.S. acknowledges the financial support from the Spanish Ministry of Science and Innovation under Project No. FIS2009-09898.

¹J. J. Loiseau, W. Michiels, S. I. Niculescu, and R. Sipahi, *Topics in Time Delay Systems: Analysis, Algorithms, and Control* (Springer, Berlin, 2009).

²F. M. Atay, *Complex Time-Delay Systems: Theory and Applications* (Springer, Berlin, 2010).

³M. Lakshmanan and D. V. Senthilkumar, *Dynamics of Nonlinear Time-Delay Systems* (Springer, Berlin, 2010).

- ⁴A. Ahlborn and U. Parlitz, *Phys. Rev. E* **72**, 016206 (2005).
- ⁵E. M. Shahverdiev and K. A. Shore, *Phys. Rev. E* **77**, 057201 (2008).
- ⁶S. Gakkhar, K. Negi, and S. K. Sahani, *Commun. Nonlinear Sci. Numer. Simul.* **14**, 850 (2009).
- ⁷A. Englert, W. Kinzel, Y. Aviad, M. Butkovski, I. Reidler, M. Zigzag, I. Kanter, and M. Rosenblum, *Phys. Rev. Lett.* **104**, 114102 (2010).
- ⁸A. Englert, S. Heiligenthal, W. Kinzel, and I. Kanter, *Phys. Rev. E* **83**, 046222 (2011).
- ⁹W. S. Lee, J. G. Restrepo, E. Ott, and T. M. Antonsen, *Chaos* **21**, 023122 (2011).
- ¹⁰S. Gakkhar and A. Singh, *Commun. Nonlinear Sci. Numer. Simul.* **17**, 914 (2012).
- ¹¹R. Martinenghi, S. Rybalko, M. Jacquot, Y. K. Chembo, and L. Larger, *Phys. Rev. Lett.* **108**, 244101 (2012).
- ¹²P. S. Landa and P. V. E. McClintock, *J. Phys. A* **33**, L433 (2000).
- ¹³S. Jeyakumari, V. Chinnathambi, S. Rajasekar, and M. A. F. Sanjuan, *Phys. Rev. E* **80**, 046608 (2009).
- ¹⁴S. Rajasekar, K. Abirami, and M. A. F. Sanjuan, *Chaos* **21**, 033106 (2011).
- ¹⁵E. Ullner, A. Zaikin, J. Garcia-Ojalvo, R. Bascones, and J. Kurths, *Phys. Lett. A* **312**, 348 (2003).
- ¹⁶J. H. Yang and X. B. Liu, *J. Phys. A* **43**, 122001 (2010).
- ¹⁷J. H. Yang and X. B. Liu, *Chaos* **20**, 033124 (2010).
- ¹⁸C. Jeevarathinam, S. Rajasekar, and M. A. F. Sanjuan, *Phys. Rev. E* **83**, 066205 (2011).
- ¹⁹D. Hu, J. H. Yang, and X. B. Liu, *Commun. Nonlinear Sci. Numer. Simul.* **17**, 1031 (2012).
- ²⁰A. Daza, A. Wagemakers, S. Rajasekar, and M. A. F. Sanjuan, *Commun. Nonlinear Sci. Numer. Simul.* **18**, 411 (2013).
- ²¹J. H. Yang and X. B. Liu, *Phys. Scr.* **82**, 025006 (2010).
- ²²J. Li and L. Zeng, *J. Phys. A* **43**, 495002 (2010).
- ²³F. C. Moon and P. J. Holmes, *J. Sound Vib.* **65**, 275 (1979).
- ²⁴J. E. Berger and G. Nunes, Jr., *Am. J. Phys.* **65**, 841 (1997).
- ²⁵A. Namajunas, K. Pyragas, and A. Tamasevicius, *Phys. Lett. A* **204**, 255 (1995).
- ²⁶A. Prasad, S. K. Dana, R. Karnatak, J. Kurths, B. Blasius, and R. Ramaswamy, *Chaos* **18**, 023111 (2008).
- ²⁷K. Srinivasan, D. V. Senthilkumar, K. Murali, M. Lakshmanan, and J. Kurths, *Chaos* **21**, 023119 (2011).
- ²⁸L. A. Pipes and L. R. Harvill, *Applied Mathematics for Engineers and Physicists*, 3rd ed. (McGraw-Hill, New York, 1970).
- ²⁹C. Yao and M. Zhan, *Phys. Rev. E* **81**, 061129 (2010).
- ³⁰B. W. Knight, *J. Gen. Physiol.* **59**, 734 (1972).
- ³¹P. Bak, C. Tang, and K. Wiesenfeld, *Phys. Rev. A* **38**, 364 (1988).
- ³²G. Golomb and G. B. Ermentrout, *Network Comput. Neural Syst.* **11**, 221 (2000).
- ³³G. Saxena, A. Prasad, and R. Ramaswamy, *Phys. Rev. E* **82**, 017201 (2010).